Applied Catalysis B: Environmental 127 (2012) 246–254

Contents lists available at SciVerse ScienceDirect

Applied Catalysis B: Environmental

journal homepage: www.elsevier.com/locate/apcatb

Catalytic combustion of chlorobenzene on the Ln modified Co/HMS

Wei Zhao[a], Jie Cheng[b], Lina Wang[a], Jinlong Chu[a], Jinkui Qu[a], Yahui Liu[a], Shaohua Li[a], Hui Zhang[a], Jianchong Wang[a], Zhengping Hao[b,*], Tao Qi[a,*]

[a] Institute of Process Engineering, Chinese Academy of Sciences, Beijing, 100190, PR China
[b] Research Center for Eco-Environmental Sciences, Chinese Academy of Sciences, Beijing, 100085, PR China

ARTICLE INFO

Article history:
Received 28 February 2012
Received in revised form 20 July 2012
Accepted 21 August 2012
Available online 28 August 2012

Keywords:
Chlorobenzene
Catalytic combustion
HMS
Rare earths

ABSTRACT

Lanthanide (Ln, including La, Ce and Nd) modified Co/HMS was prepared via two pathways: extra-framework modified post-loading and framework modified direct synthesis. The influence of modified methods, rare earths kind and rare earths loading on the catalytic performance of Co/HMS was studied by the catalytic combustion of chlorobenzene (CB). It was found that the extra-framework Ce modified catalysts show the better catalytic performance than the framework Ln modified ones due to that the forming of CeO_2 is advantaged to obtain the fine Co_3O_4 crystal clusters and the reduction of Ce^{4+} ions to Ce^{3+} species probably will promote neighboring reduction of Co species. The suitable extra-framework Ce loading (6%, mass fraction) can effectively ameliorate the redox ability of Co species in the channel of HMS. Since the channel of HMS itself and $Co(NO_3)_3{\cdot}6H_2O$ aqueous solution both are hydrophilic, the polarity adjusting function of framework Ln to the internal reaction between Co species and support is not great in this case. However, the slightly improved redox ability and weak acidity originated from framework Ln still can do some contribution to the catalytic performance. The electronic structure of Co and Ce is advantageous to the delocalization of π-electrons and the forming of radical species.

1. Introduction

Chlorinated volatile organic compounds (Cl-VOCs) have been considered potent environmental pollutants due to their direct hazards on human health and indirect effects on the depletion of ozone layer [1]. Since Cl-VOCs are released to the atmosphere from a wide range of industrial processes and the incineration of municipal and medical wastes, highly desirable to develop effective methods for the decomposition and removal of chlorinated organic compounds prior to their release into the environment. At present, the main industrial process for Cl-VOCs destruction involves thermal combustion at extremely high temperatures (850–1000 °C). This is a rather expensive process and also lead to highly toxic byproducts, such as dioxins and dibenzofurans formed by incomplete combustion [2]. Catalytic combustion is one of the most promising technologies for the removing of volatile organic compounds. The major advantage of this technology is that combustion can be performed at low temperatures (<500 °C) and much dilute pollutants (<1000 ppm) which cannot be thermally combusted without additional fuel [3]. About the catalysts for Cl-VOCs catalytic combustion, most report have focused on three types of catalysts based on noble metals [4,5], transition metals [6,7] and zeolites [8,9]. Generally, supported noble metal catalysts exhibit higher catalytic activities compared with other two catalysts. However, the disadvantages of noble metal catalysts include: (a) their higher costs, (b) deactivation due to their sensitivity to poisons from waste gases, (c) causing chlorination of organic compounds besides oxidation [10]. The activities of zeolite catalysts are usually originated from their acid properties. However, the problem of the formation of by-product (polychlorinated compounds) on these catalysts is yet to be solved [11]. Transition metal oxide catalysts not only can resist the deactivation caused by chlorine poisoning but also can enhance catalytic activities themselves by modifying with other active elements or by loading onto some support whose acid–base properties can be adjusted [12,13]. HMS mesoporous molecular sieve whose channel is wormhole like rather than straight like can be synthesized at ambient temperature in a short time and its template is commercially available and recoverable. These characterizations provide it some advantages compared to M41s mesoporous molecular sieves based on large-scale industrial application [14]. Rare-earth elements have been widely used in the field of catalysis. They can participate in the stabilization of supports against thermal sintering and enhance the performance of catalysts in storing and releasing oxygen as well as reducing the reaction activation energy [15,16]. In this paper, we studied the influence of rare-earth elements on Co/HMS catalysts for the catalytic combustion of chlorobenzene from two ways: one is incorporating Ln into the framework of HMS; the other is introducing Ln

* Corresponding authors. Tel.: +86 10 82627090; fax: +86 10 62631710.
E-mail addresses: zpinghao@rcees.ac.cn (Z. Hao), tqi@home.ipe.ac.cn (T. Qi).

0926-3373/$ – see front matter © 2012 Elsevier B.V. All rights reserved.
http://dx.doi.org/10.1016/j.apcatb.2012.08.019

in the channel (extra-framework) of HMS. It was found that the extra-framework Ce modified Co/HMS catalysts show the better catalytic performance than the framework Ln modified ones. The suitable extra-framework Ce loading (6%, mass fraction) can effectively ameliorate the redox ability of Co species in the channel of HMS. The polarity adjusting function of framework Ln to the internal reaction between Co species and support is not great in our test system.

2. Experimental

2.1. Catalysts preparation

The tetraethyl orthosilicate (TEOS), dodecylamine (DDA), ethanol (EtOH), lanthanum nitrate ($La(NO_3)_3{\cdot}6H_2O$), cerium nitrate ($Ce(NO_3)_3{\cdot}6H_2O$), neodymium nitrate ($Nd(NO_3)_3{\cdot}6H_2O$), cobalt nitrate ($Co(NO_3)_3{\cdot}6H_2O$), manganese nitrate ($Mn(NO_3)_3$, 50 wt%), palladium chlorides and chlorobenzene were purchased from the No. 1 Chemical Reagent Company of Beijing. Deionized water was used throughout this study.

In a typical preparation, the mixture solution of TEOS, EtOH and lanthanide nitrates was added under vigorous stirring to a solution of DDA in ethanol and deionized water. The molar ratio of this synthesis mixture was 1.0 SiO_2:0.01 lanthanide nitrates: 0.2–0.4 DDA:7–10 EtOH:142 H_2O (for the synthesis of pure HMS, lanthanide nitrates is not added here). This mixture was aged at ambient temperature for 24 h. The as-synthesized Ln-HMS were filtered, washed with H_2O, air-dried at 70 °C and calcined in air at 550 °C for 5 h. Ln nitrate salts and active species (Pd, metal oxides) were loaded onto the HMS (or Ln-HMS) via the wetness impregnation method and the weight percent of metal atom to the support was used as unit (e.g. HMS loaded 6 wt% of Co was denoted as Co6/HMS). The impregnated solids were calcined in air at 500 °C for 3 h (for Pd/HMS catalyst, the sample was then reduced in hydrogen at 400 °C for 1 h).

2.2. Characterization

Powder X-ray diffraction (XRD) patterns were collected on Bruker D5005 diffractometer using Cu K_α radiation (λ = 1.5418 Å; 40 kV and 40 mA), Ni filter, scan speed 4°/min. Nitrogen adsorption–desorption isotherms were obtained on a NOVA1200 gas sorption analyzer. The mesopore size distributions were derived from the desorption branch of the N_2 isotherms using the Barrett–Joyner–Halenda (BJH) method. The total pore volumes were estimated from the amount of nitrogen adsorbed at a relative pressure (P/P_0) of ca. 0.99. The diffuse reflectance UV–vis spectra were collected on a HITACHI UV3000 scanning spectrophotometer from 190 to 800 nm. The powder sample was loaded into a quartz cell and $BaSO_4$ was used as reference. Temperature-programmed reduction (TPR) and oxidation (TPO) were performed for catalysts on a conventional TPR/TPO apparatus equipped with a thermal conductivity detector (TCD). Prior to each TPR run, the catalyst (30 mg) was pretreated at 300 °C under an Ar flow (30 ml/min) for 30 min. The catalyst was then heated from room temperature to 800 °C at a constant heating rate of 10 °C/min using H_2 (5 vol%)/He (95 vol%) under a flow rate of 30 ml/min. H_2 concentration was monitored by the TCD detector. TPO test was conducted with O_2 (4 vol%)/He (96 vol%) mixed gas at a flow rate of 50 ml/min. In each run, after the blowing of Ar at 300 °C for 1 h, the temperature was raised from room temperature to 800 °C at a constant heating rate of 10 °C/min. XPS spectra were recorded on the Thermo ESCALAB 250 electron spectrometer with base pressure 1×10^{-8} Pa. The energy positions of photoelectron line were determined with respect to the reference C 1s line (BE 284.8 eV).

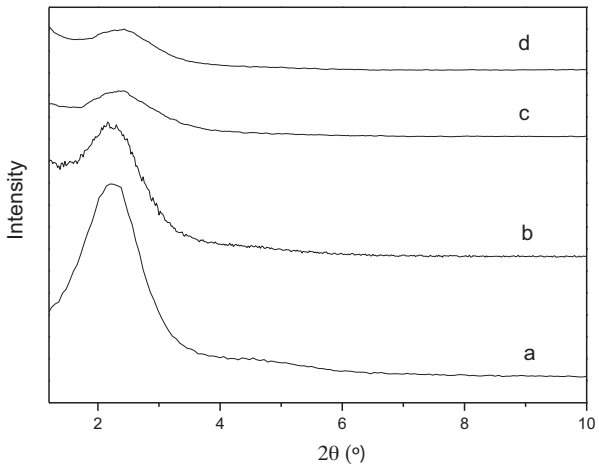

Fig. 1. Low angle XRD patterns of modified HMS samples (a) HMS; (b) Pd0.9/HMS; (c) Co6/HMS; (d) Mn6/HMS.

2.3. Catalytic combustion reaction

Catalytic activity tests were performed in a continuous-flow fixed-bed reactor of 6 mm i.d. using 0.1 g catalyst. To create the stream containing 1000 ppm chlorobenzene, one stream of pure air was passed through a boat-shape saturator in an ice-bath to get a mixed gas containing high concentration chlorobenzene and then it was diluted with another stream of pure air before reaching the catalyst bed. The gas hourly space velocity (GHSV) in the tests was kept ca. 30,000 h^{-1}. An on-line gas chromatograph equipped with FID detector and a Ni catalyst converter which was used for converting CO_2 quantitatively into methane before the detector was used to analyze the concentration of chlorobenzene and CO_2 in the inlet and outlet gas. Within the application limits of FID, the carbon balance gives 5–10% less amount in the outlet stream than in the inlet stream in each catalytic evaluation and this fact means that only a few deposition of C species occurs on the surface of catalysts.

3. Results and discussion

3.1. Characterization of HMS supported by different active species

Fig. 1 is the XRD patterns of HMS loaded with different active species. You can see that all the modified HMS samples keep the [1 0 0] diffraction peak although the intensity of this peak decreases obviously according to the order of 0.9Pd/HMS > Co6/HMS ≈ Mn6/HMS. It means the two-dimensional hexagonal mesostructure (p6m) of HMS still exists. The nitrogen adsorption–desorption results of modified HMS samples show that the wetness impregnation procedure can cause some lose of surface area and pore volume (Table 1). However, the maximum lose of surface area is less than 18% (Mn6/HMS) which is not enough to change the type IV isotherms of modified HMS samples (Fig. 2).

Fig. 3 is the TPR results of Co6/HMS and Mn6/HMS. Just as we know, the reduction of supported cobalt oxide was generally divided into two stages [17,18]: the reduction of large crystalline Co_3O_4 particles at lower temperature (<500 °C) and the reduction of surface cobalt oxide species that interact with the support at higher temperature (>500 °C). For Co6/HMS sample (Fig. 3a), there are two main reduction peaks at 322 °C and 396 °C which usually assigned to the reduction of Co_3O_4 to CoO and the subsequent reduction of CoO to Co^0 [19,20], respectively below 450 °C. Beginning at 450 °C, a broad reduction peak is observed, suggesting the presence of surface cobalt species that interact with the support [21]. For Mn6/HMS sample (Fig. 3b), there exist a main peak at

Table 1
Surface area and porous structure of HMS samples under investigation.

Samples	SA (m^2/g)[a]	V_p (cm^3/g)[b]	Particle size of Co_3O_4 (nm)
HMS	869.7	0.75	–
Pd0.9/HMS	862.9	0.74	–
Mn6/HMS	713.6	0.59	–
Co6/HMS	788.2	0.64	11.5
Ce1.5-Co6/HMS	715.2	0.60	11.7
Ce3-Co6/HMS	693.6	0.58	11.6
Ce6-Co6/HMS	**653.8**	**0.53**	**10.5**
Ce9-Co6/HMS	634.6	0.49	9.3
La6-Co6/HMS	**688.5**	**0.50**	**11.9**
Nd6-Co6/HMS	**667.2**	**0.46**	**13.1**
Co6/La-HMS	495.6	0.57	–
Co6/Ce-HMS	688.8	0.83	9.9
Co6/Nd-HMS	650.6	0.69	9.2

[a] SA: surface area.
[b] V_p: pore volume

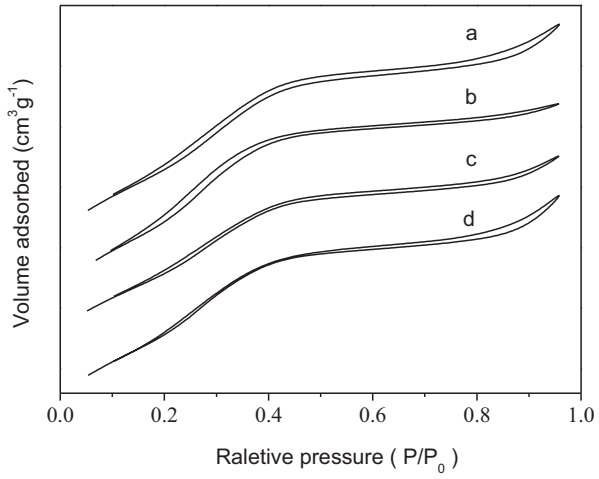

Fig. 2. Nitrogen adsorption–desorption results of modified HMS samples (a) HMS; (b) Pd0.9/HMS; (c) Co6/HMS; (d) Mn6/HMS.

325 °C and a shoulder peak at 412 °C. About these two peaks, which was based on the H_2-TPR profile of pure MnOx (there are two overlapped strong reduction peaks at 380 and 480 °C, respectively) and Kapteijn and Arena' work [22,23], Wu et al. [24] proposed that the peak at lower temperature could be assigned to the reduction of MnO_2/Mn_2O_3 to Mn_3O_4, while the peak at higher temperature corresponds to the reduction of Mn_3O_4 to MnO.

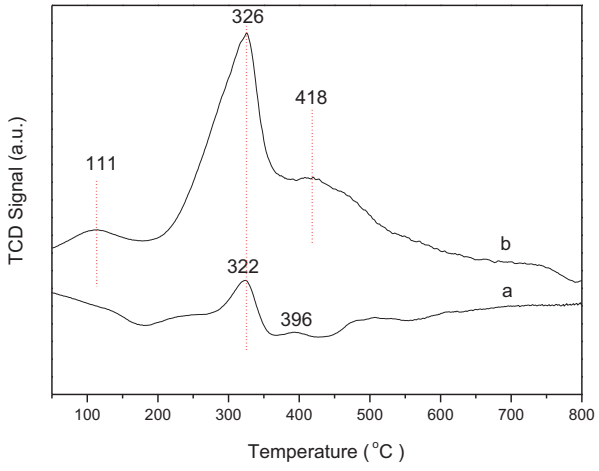

Fig. 3. H_2-TPR profiles of modified HMS samples (a) Co6/HMS; (b) Mn6/HMS.

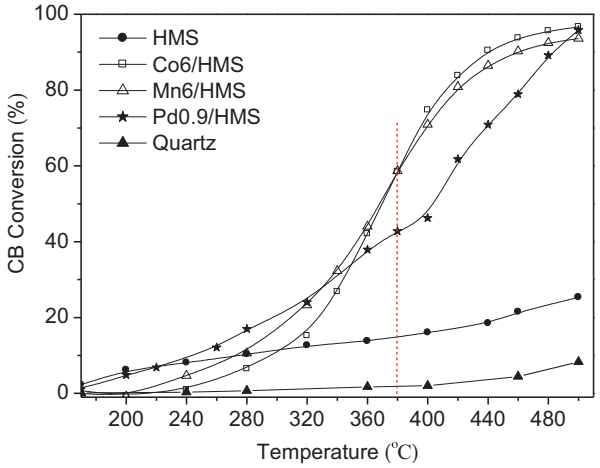

Fig. 4. Conversion curves of chlorobenzene catalytic combustion over different catalysts.

3.2. Catalytic performance of supported HMS

The conversion curves of chlorobenzene catalytic oxidation over different catalysts were shown in Fig. 4 and the catalytic activity was shown in Table 2. It was found: (1) for the high temperature activity (90% conversation of chlorobenzene), the Co6/HMS is the best one among three catalysts (the needed temperature is 440 °C). (2) For the low temperature activity (10% conversation of chlorobenzene), Pd0.9/HMS is the best one (the needed temperature is 240 °C). (3) More interesting, 380 °C (corresponding conversation of chlorobenzene is 60%) seems like a boundary for Co6/HMS and Mn6/HMS two transition metal oxide catalysts. When the reaction temperature is below this point, Mn6/HMS catalyst show the better activity compared to Co6/HMS catalyst. On the contrary, if the reaction temperature is above this point, the case is converse. From above TPR results, we found the beginning temperature of 325 °C peak of Mn6/HMS sample is lower than that of Co6/HMS and the H_2 consumed quantity of this peak is much higher than that of Co6/HMS. Thus, we thought Mn6/HMS would have better redox properties than Co6/HMS in this temperature region. In other words, Mn6/HMS will have better catalytic performance than Co6/HMS at this time. While, for the second reduction peak, the temperature is 396 °C of Co6/HMS which is obviously lower than that of Mn6/HMS (418 °C) although its H_2 consumed quantity is less than that of Mn6/HMS. In this case, since the C—Cl bond has been activated partly under high temperature

Table 2
The catalytic performance of different catalysts.

Catalysts	T_{10} (°C)[a]	T_{50} (°C)[a]	T_{90} (°C)[a]
Quartz	>500	>500	>500
HMS	270	>500	>500
Pd0.9/HMS	240	405	490
Co6/HMS	300	370	440
Mn6/HMS	270	370	470
Co_3O_4	240	390	>500
Ce1.5-Co6/HMS	320	380	460
Ce3-Co6/HMS	290	360	440
Ce6-Co6/HMS	**230**	**350**	**440**
Ce9-Co6/HMS	290	365	440
La6-Co6/HMS	**290**	**380**	**470**
Nd6-Co6/HMS	**280**	**410**	**>500**
Co6/La-HMS	300	380	460
Co6/Ce-HMS	290	380	450
Co6/Nd-HMS	300	380	460

[a] T_{10}, T_{50} and T_{90} were the temperatures at which 10%, 50% and 90% of chlorobenzene were converted.

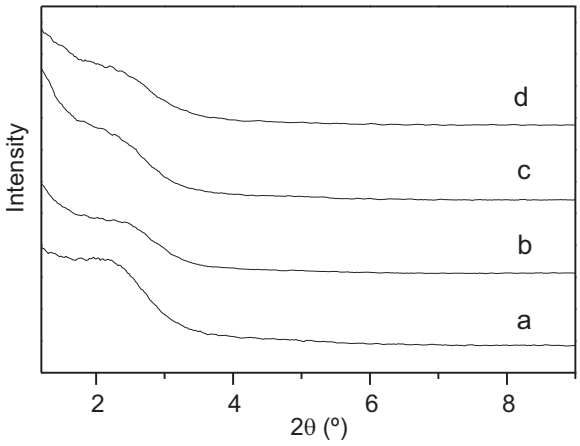

Fig. 5. Low angle XRD patterns of extra-framework Ce modified Co6/HMS samples (a) Ce1.5-Co6/HMS; (b) Ce3-Co6/HMS; (c) Ce6-Co6/HMS; (d) Ce9-Co6/HMS.

condition (>380 °C) we speculated that the redox ability of active sites (Co6/HMS > Mn6/HMS) play much more important role than the number of active sites (Co6/HMS < Mn6/HMS). Based on above discussion, we selected Co6/HMS as our target catalyst and studied the influence of Ln on it.

3.3. Characterization of extra-framework Ln modified Co/HMS

Ceria has been widely used as a direct support material or an additive in many oxidation catalysts because of its low temperature reducibility, oxygen storage and release properties which originate from its one-electron oxidation and existence of different cerium ions sites [25,26]. In addition, low decomposition temperature (450 °C) of $Ce(NO_3)_3{\cdot}6H_2O$ is also an advantage of ceria. Thus, we first studied the influence of extra-framework Ce amount on the Co6/HMS catalyst.

Figs. 5 and 6 are the low angle XRD and N_2 adsorption results of extra-framework Ce modified Co/HMS. We can see that all the four samples keep the typical type IV isotherms although their [1 0 0] diffraction peak in low angle XRD patterns lose greatly. Table 1 gives us more detail information. As the Ce loading increases, surface area and pore volume of Ce modified Co/HMS decrease distinctly (the maximum decrease of surface area and pore volume is 19.5% and 23.4%, respectively). Especially, if the Ce loading increases from 3 wt% to 6 wt%, both the low angle XRD and N_2 adsorption data become worse sharply. Obviously, the increased extra-framework Ce amount will cause the physic characterization deterioration of Co6/HMS catalyst. As followed, we studied the high angle XRD results (Fig. 7) of Ce modified Co/HMS to check crystal states of Ce oxide and Co oxide. It was found that the intensity of the diffraction peaks (37 °C) belonged to the Co_3O_4 decreases a little as the extra-framework Ce mount increases from 1.5 wt% to 9 wt%. However, the width of this peak becomes wider when the Ce mount is above 6 wt%. Meanwhile, the diffraction peaks belonging to CeO_2 appears distinctly at this time. This means that the emergence of CeO_2 crystal clusters would cause decrease in the size of Co_3O_4 crystal clusters (based on the Scherrer formula, $D = K\lambda/\beta\cos\theta$, where D is the average particle size (nm), K is the Scherrer constant, λ is the wavelength of X-ray source, β is the full width at half-maximum and θ is the Bragg's angle [27]; Table 1). In order to study the influence of these two crystal clusters on the catalysts redox ability, we studied the TPR tests of these catalysts.

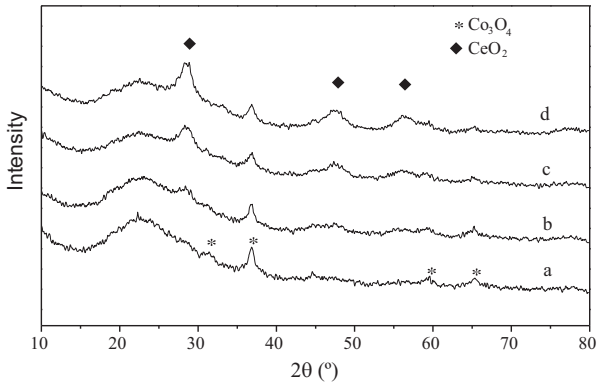

Fig. 7. High angle XRD patterns of extra-framework Ce modified Co6/HMS samples (a) Ce1.5-Co6/HMS; (b) Ce3-Co6/HMS; (c) Ce6-Co6/HMS; (d) Ce9-Co6/HMS.

From Fig. 8, we found that the TCD signals change severely when the Ce mount increases from 1.5 wt% to 9 wt%. It suggests that extra-framework Ce can influence the redox ability of Co6/HMS catalyst greatly. As the extra-framework Ce amount increases, not only the 325 °C peak shifts to the low temperature region but also its H_2 consumed quantity increases obviously. If the Ce mount is above 6 wt%, a new TCD signal emerges at 436 °C. The shifting of 325 °C peak to the low temperature region probably is related to the low temperature reducibility of CeO_2. While the high H_2 consumed quantity of Ce modified Co6/HMS catalyst could be ascribed to that the

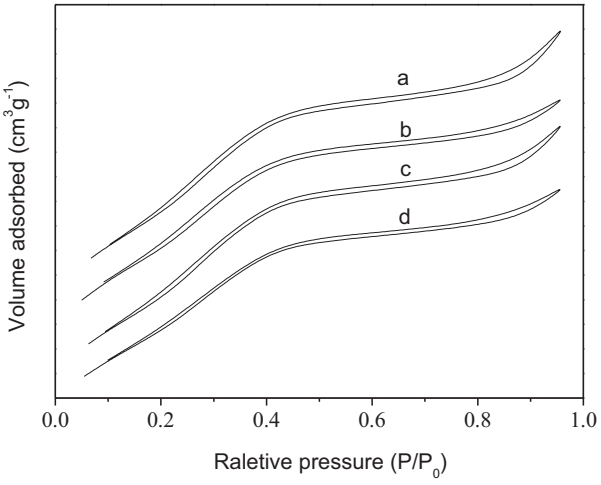

Fig. 6. Nitrogen adsorption–desorption results of extra-framework Ce modified Co6/HMS samples (a) Ce1.5-Co6/HMS; (b) Ce3-Co6/HMS; (c) Ce6-Co6/HMS; (d) Ce9-Co6/HMS.

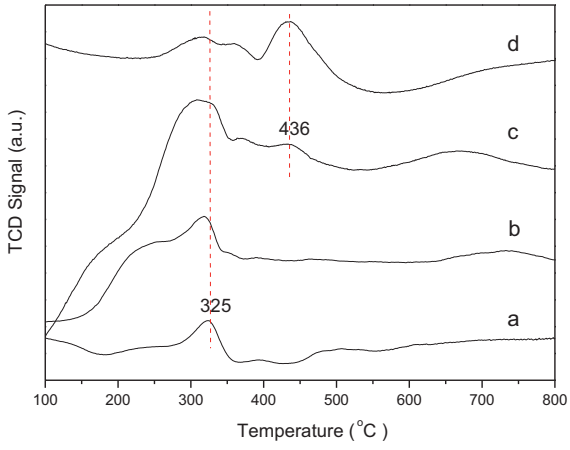

Fig. 8. H_2-TPR profiles of extra-framework Ce modified Co6/HMS samples (a) Ce1.5-Co6/HMS; (b) Ce3-Co6/HMS; (c) Ce6-Co6/HMS; (d) Ce9-Co6/HMS.

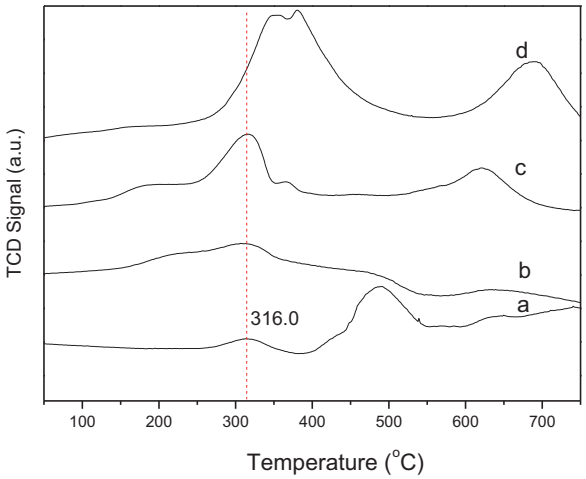

Fig. 9. H_2-TPR profiles of used extra-framework Ce modified Co6/HMS samples (a) Ce1.5-Co6/HMS; (b) Ce3-Co6/HMS; (c) Ce6-Co6/HMS; (d) Ce9-Co6/HMS.

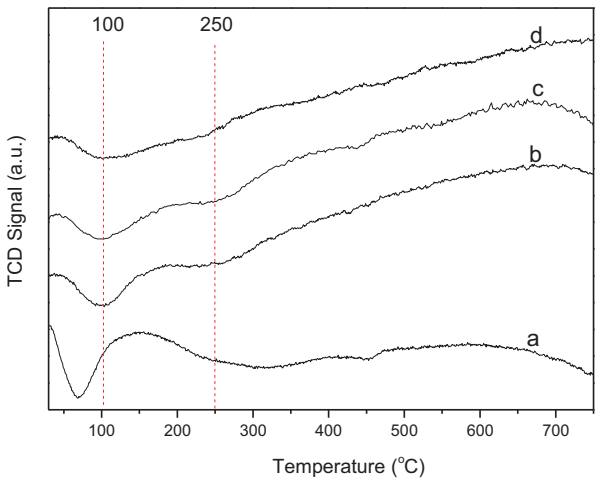

Fig. 10. TPO profiles of fresh extra-framework Ce modified Co6/HMS samples after H_2-TPR tests (a) Ce1.5-Co6/HMS; (b) Ce3-Co6/HMS; (c) Ce6-Co6/HMS; (d) Ce9-Co6/HMS.

appearing of Ce species will be advantaged to form the fine Co_3O_4 crystal clusters, thus, much more Co_3O_4 can be reduced by H_2 compared to the large size Co_3O_4 particles. This result corresponds well to the above high angle XRD results. About the new signal at 436 °C, we spectacled that the appearance of this signal would be related to the Ce^{4+} ions which also undergo a reduction to Ce^{3+} species [28] since Ce species can be highly dispersed on the surface of HMS too and the neighboring Co species reduction can either promote this procedure.

Compared to the H_2-TPR spectra of fresh catalysts, the used catalysts have different changes depending on several samples (Fig. 9). For Ce1.5-Co6/HMS catalyst, the intensity of ca.325 °C peak decreases obviously while that of ca.500 °C peak increases evidently. It means that the interaction between surface cobalt species and support enhances after the catalytic test. The probable reason of this fact is that the part of surface cobalt species could combine with the water (originated from the combustion of CB) to form the hydrated Co oxide/cobalt hydroxide and then, these hydrated Co oxide/cobalt hydroxide species would react to the hydroxyl (OH group) of support to form Co—O—Si bond subsequently. About the Ce3–Co6/HMS catalyst, the increased amount of Ce species seems inhibiting the interaction between cobalt species and support. As a result, the ca. 500 °C peak almost disappears in this case. The sharp intensity decrease of the peak before 350 °C could also ascribe to the forming of hydrated Co oxide/cobalt hydroxide. Further raising the Ce amount to 6 wt%, the changes of TCD signal related to the Co species (before 350 °C) are relatively insignificant (just a few decreased intensity). However, both the disappearing of 436 °C peak and the intensity increase of ca.650 °C peak suggest that Ce species would substitutes Co species to react with support prior at this time. Regarding the Ce9-Co6/HMS catalyst, a combined strong peak centered at 370 °C and a ca. 680 °C peak whose intensity is higher than that of the ca. 650 °C peak for Ce6-Co6/HMS catalyst appear. The existence of enough Ce species one aspect would be advantagious to the forming of CoO (partly reduction of Co_3O_4) during the catalytic combustion reaction and the other aspect is that it could provide more Ce species to combine with the hydroxyl support (occupy more OH sites). Thus, the TPR signal related to the reduction from CoO to Co and the TPR signal reflecting the interaction between Ce species and support become stronger.

Fig. 10 is the TPO profiles of fresh catalysts after H_2-TPR reduction procedure. Only the negative peaks appear in all four tested samples and the intensity of negative peak decreases as the Ce amount enhances. The emerging of negative peaks suggests that the increase of O_2 concentration or the forming of other gas without the consumption of O_2 happens during the test process. As the position of negative peaks are below 100 °C and the TPO test were performed after the blowing of Ar at 300 °C for 1 h, we did not think that the decomposition of oxides (did not reduce completely in TPR test) to release O_2 and the desorption of physic adsorbed H_2 in TPR test are the reasonable explanation for these results. Thus, the possible reason will be that some chemic adsorbed H_2 in TPR test will be desorbed in the flow of O_2/He due to the activity of O_2. Since Ce oxide species itself has certain reducibility, its existence will be disadvantagious to the chemic adsorption of H_2. Therefore, the enhanced Ce amount will causes the reduction of chemic adsorbed H_2, and then, the desorbed H_2 will decrease in TPO tests.

3.4. Catalytic performance of extra-framework Ln modified Co/HMS

The catalytic performance of extra-framework Ce modified Co/HMS was shown in Fig. 11 and Table 2. We found the low temperature activity (T_{10} temperature) of Co/HMS catalyst is improved obviously (T_{10} temperature decreases from 300 °C to 230 °C) when Ce mount increases from 1.5 wt% to 6 wt% while the improvement of high temperature

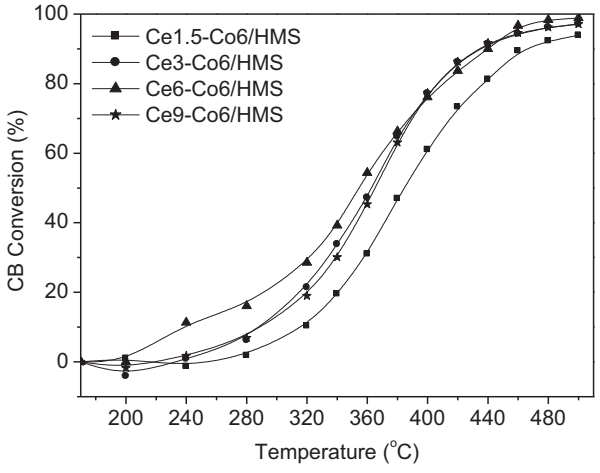

Fig. 11. Conversion curves of chlorobenzene catalytic combustion over extra-framework Ce modified Co6/HMS.

activity (T_{50} and T_{90} temperature) is limited. When the mount of Ce increases from 6 wt% to 9 wt%, both low temperature activity and high temperature activity became worse.

Seen from Fig. 8, we knew the H_2-TPR signal of Ce1.5-Co6/HMS is similar to that of Co6/HMS however its XRD pattern and nitrogen adsorption data are obviously weaken to that of Co6/HMS. Thus, we thought when extra-framework Ce amount is not enough (1.5 wt %) its beneficial role for active sites could not compensate its disadvantageous role for diffusion speed. As a result, its catalytic performance is worse than that of Co6/HMS. Continuously increasing extra-framework Ce amount to 6 wt%, both 325 °C peak shifts to the low temperature region and the H_2 consumed quantity increase (H_2-TPR results) illustrate that redox ability of Co6/HMS had been improved actually. At this time, the beneficial role of extra-framework Ce for active sites will overwhelm its disadvantageous role for diffusion speed, thus the best catalytic activity will be obtained. Of course, we could not neglect the contribution of CeO_2 crystal clusters to the improvement of thermal conductivity and heat transmitting ability for catalysts in this case. Further enhancing extra-framework Ce amount to 9 wt%, the H_2-TPR results demonstrate the redox ability of Co6/HMS does not improve accordingly and even retrogresses since the existing of overmuch CeO_2 crystal clusters not only could not promote the redox ability of Co species but would impede it due to H_2 consumption by itself. Owing to the aggravated diffusion speed problem, the catalytic performance of Ce9-Co6/HMS becomes worse compared to Ce6-Co6/HMS.

Although the decomposition temperatures of $La(NO_3)_3{\cdot}6H_2O$ and $Nd(NO_3)_3{\cdot}6H_2O$ are much higher than 500 °C, in order to study the influence of different extra-framework Ln states on the catalytic performance of Co6/HMS catalyst, we still calcined these two Ln modified Co/HMS samples at 500 °C keeping 6 wt% loading. From chlorobenzene conversion curves (Fig. 12 and Table 2), we found the order of catalytic activity of three catalysts is: Ce6-Co6/HMS > La6-Co6/HMS > Nd6-Co6/HMS no matter about the low temperature activity and the high temperature activity. Moreover, the high temperature activity of La6-Co6/HMS and Nd6-Co6/HMS is even worse than that of Co6/HMS (Especially, Nd6-Co6/HMS catalyst cannot get the 90% conversion of chlorobenzene at 500 °C). Since low angle XRD (Supplementary file, Fig. 1) and N_2 adsorption results (Table 1) among three samples have not the obvious difference, we believed that the existence of Ln salts (La6-Co6/HMS and Nd6-Co6/HMS do not show the diffraction peaks of La oxide and Nd oxide in high angle XRD spectra, Supplementary file, Fig. 2) is disadvantagious to the catalytic activity of Co6/HMS in high temperature region. The reason probably is that the crystal water of $La(NO_3)_3{\cdot}6H_2O$ and $Nd(NO_3)_3{\cdot}6H_2O$ will be released in high temperature condition and this water molecule can reduce the activity

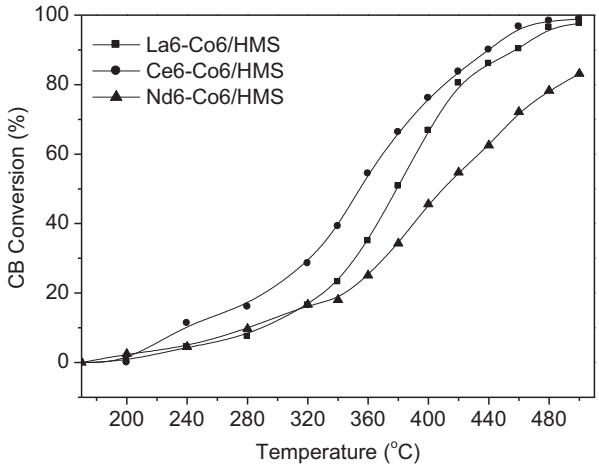

Fig. 12. Conversion curves of chlorobenzene catalytic combustion over extra-framework Ln modified Co6/HMS.

of Co6/HMS via a competitive adsorption path to block a number of active sites, and hence, inhibit the rate of the reaction [29]. Since there are two crystal water of $Nd(NO_3)_3{\cdot}6H_2O$ are hydrogen bond type (which is less stable as compared to co-operated bond type) while $La(NO_3)_3{\cdot}6H_2O$ only has one, thus, the activity of Nd6-Co6/HMS is worse than that of La6-Co6/HMS.

3.5. Characterization of framework Ln modified Co/HMS

Fig. 13 is the low angle XRD and UV–visible results of framework Ln modified HMS samples (Ln-HMS). All modified HMS samples keep the [100] peaks belonging to p6m whereas the intensity of this peak decreases clearly as compared to that of pure HMS. The fact that 216 nm peak appears in the Ce-HMS and Nd-HMS but not in La-HMS suggests that Ce and Nd element has been successfully introduced into the framework of HMS. After loading of Co_3O_4 on the Ln-HMS, their XRD patterns become much worse (Fig. 14). However, their nitrogen adsorption–desorption results (Fig. 15) indicate that all of them keep the typical type IV isotherms although the hysteresis loop between $P/P_0 = 0.4$ and $P/P_0 = 1.0$ become substantial which may be originated from the inter particle capillary condensation. The existing of inter particle capillary condensation will provide additional pore volume. Thus, the pore volume of Co6/Ce-HMS and Co6/Nd-HMS are higher than that of Co/HMS.

The high angle XRD (Fig. 16) and H_2-TPR (Fig. 17) results show that Ln element introduced into the framework of HMS does not cause great influence on the Co loading process and the following

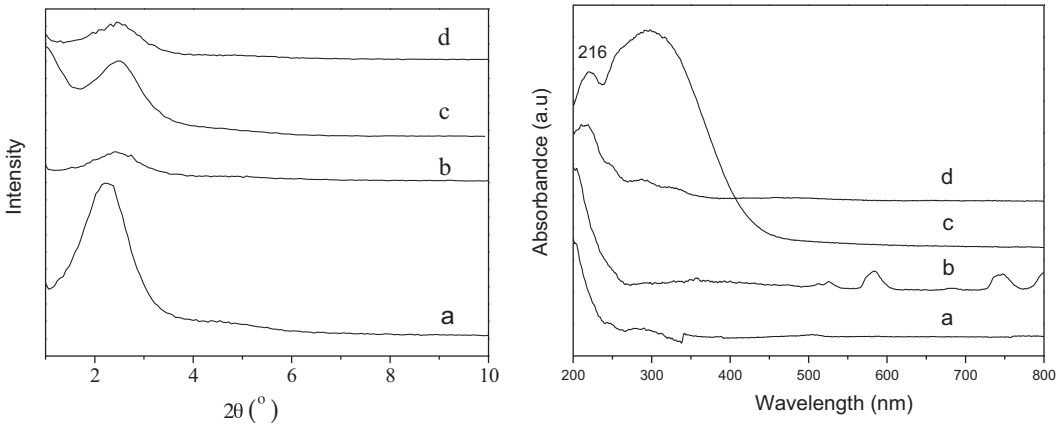

Fig. 13. Low angle XRD and UV–visible spectra of framework Ln modified HMS (a) HMS; (b) La-HMS; (c) Ce-HMS; (d) Nd-HMS.

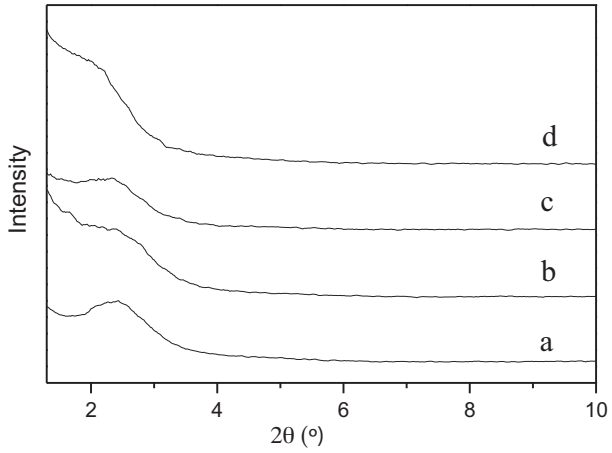

Fig. 14. Low angle XRD patterns of Co/Ln-HMS samples (a) Co6/HMS; (b) Co6/La-HMS; (c) Co6/Ce-HMS; (d) Co6/Nd-HMS.

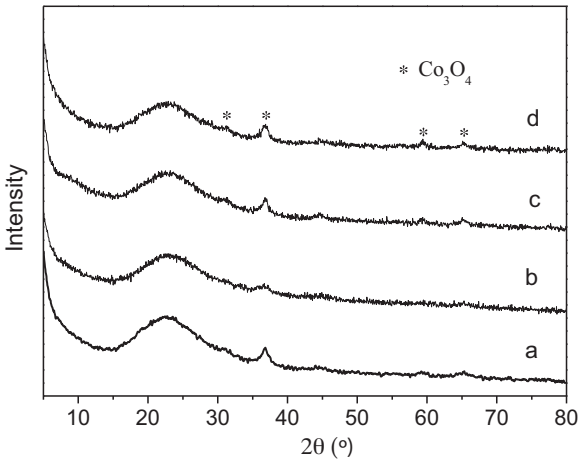

Fig. 16. High angle XRD patterns of Co/Ln-HMS samples (a) Co6/HMS; (b) Co6/La-HMS; (c) Co6/Ce-HMS; (d) Co6/Nd-HMS.

redox behavior of Co/Ln-HMS catalysts. The Co_3O_4 diffraction peaks of Co6/Ce-HMS and Co6/Nd-HMS are similar to that of Co6/HMS. However, that of Co6/La-HMS obviously is weaker. The reason is that La element has not been incorporated into the framework of HMS successfully during the synthesis procedure due to the large ion radium of La^{3+}. Thus, after filtered and washed steps, some $La(NO_3)_3{\cdot}6H_2O$ still would be left into the channel of HMS. This thermal stability extra-framework La salt (the decomposed temperature is 780 °C) is not advantagious for the decomposition of $Co(NO_3)_3{\cdot}6H_2O$.

Different from that, the extra-framework CeO_2 will cause the obvious shifting of 325 °C reduced peak towards low temperature direction in Co6/HMS H_2-TPT profiles, this reduced peak of Co6/Ln-HMS samples just slightly moves to low temperature region (except Co6/La-HMS). It means the influence of framework Ln elements on the redox ability of Co6/Ln-HMS by adjusting the internal reaction between Co species and support is not great in this system. The reason probably is that the channel of HMS itself is hydrophilic, thus, the framework modification could not improve the diffusion and distribution of hydrophilic $Co(NO_3)_3{\cdot}6H_2O$ aqueous solution greatly. If the channel is hydrophobic, the case probably will be rather different. In addition, the appearance of 780 °C reduced peak in Co6/La-HMS H_2-TPT profile will be attributed to the H_2 consumption of La_2O_3 decomposed by $La(NO_3)_3$ this time.

The XPS technique was used to determine the oxidation state of Ce and Co on the surface of Co6/HMS, Co6/Ce-HMS and Ce6-Co6/HMS. From Fig. 18 left one, you can see that the binding energy (BE) values of Co $2p_{3/2}$ core-level at ca. 780.0 eV, corresponded to the BE for Co^{2+} on CoOx [30], exists for all three samples while the BE values decrease from 780.9 eV to 780.3 eV for two Ce modified Co6/HMS samples. Moreover, the width of ca. 780.0 eV peak increases according to the order: Co6/HMS, Co6/Ce-HMS and Ce6-Co6/HMS. The shift to lower BE values of 0.6 eV for two Ce modified Co6/HMS suggest that the stability of surface Co species decreases a little due to the existence of Ce species. Usually, the decrease of surface Co species stability means the enhancing of theirs reactivity. Due to the reason that the distance between extra-frame CeO_2 and surface CoOx species is close enough and the reason that some outermost orbits energy level of Ce species match that of Co species, the existence of extra-frame CeO_2 would cause Co species forming more scattered orbits. Thus, the width of ca.780.0 eV peak is the largest in the case of Ce6-Co6/HMS. For Co6/Ce-HMS, since Ce was doped into the frame work of HMS, the distance between Ce species and Co species is not near as the above case. As a result, the broaden phenomena of ca.780.0 eV peak is weak in this case.

From Fig. 18, right one, we found that Ce 3d core level is formed by three regions: $3d_{5/2}$ (882.6 eV), $3d_{3/2}$ (898.1 eV) and the "shake-up" satellites (916.6 eV). The fact that Ce 3d level of Co6/Ce-HMS shifts slightly to the high energy region compared to that of

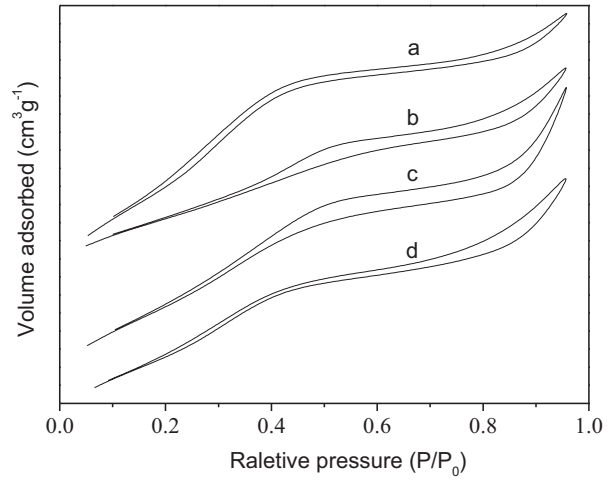

Fig. 15. Nitrogen adsorption–desorption results of Co/Ln-HMS samples (a) Co6/HMS; (b) Co6/La-HMS; (c) Co6/Ce-HMS; (d) Co6/Nd-HMS.

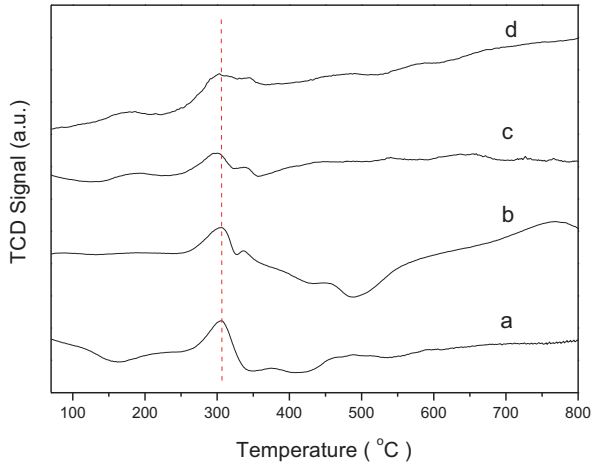

Fig. 17. H_2-TPR profiles of Co/Ln-HMS (a) Co6/HMS; (b) Co6/La-HMS; (c) Co6/Ce-HMS; (d) Co6/Nd-HMS.

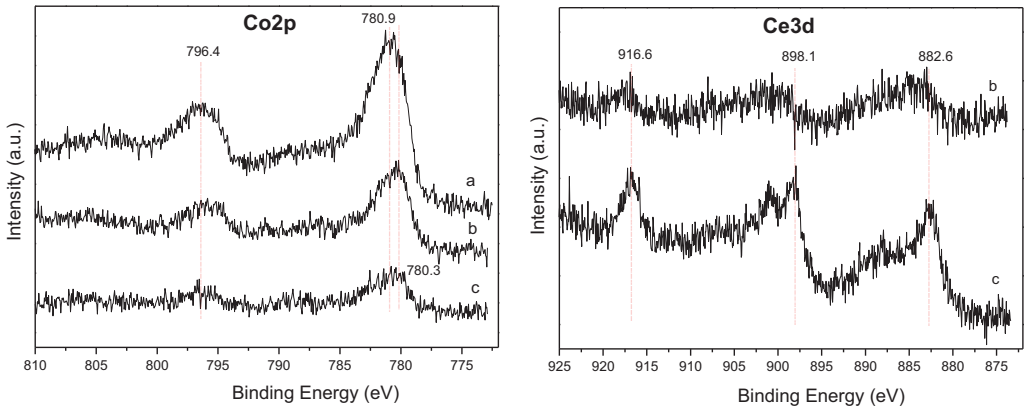

Fig. 18. XPS spectra of different catalysts (a) Co6/HMS; (b) Co6/Ce-HMS; (c) Ce6-Co6/HMS.

Ce6-Co6/HMS suggests that the stability of frame Ce is some higher than that of extra-frame Ce.

3.6. Catalytic performance of framework Ln modified Co/HMS

The conversion curves of chlorobenzene catalytic oxidation over Co6/Ln-HMS were shown in Fig. 19. It was found that four curves almost overlap from beginning to end although the curve of Co6/HMS is the best one. Since the XRD (Fig. 14) and nitrogen adsorption–desorption results (Table 1) show that the physic characterization of Co6/HMS is better than that of Co6/Ln-HMS, the similar catalytic performance between Co6/HMS and Co6/Ln-HMS suggested that the disadvantage of Co6/Ln-HMS catalyst on diffusion of substrate in catalytic reaction has been compensated by its slightly improved redox ability and weak acidity originated from its framework Ln.

3.7. Reaction mechanism for chlorobenzene combustion

Based on the above results, we tentatively proposed the following reaction mechanism:

$$Co_3O_4(CoO\text{-}Co_2O_3) + \text{Ph-Cl} \rightarrow \text{Ph-Cl}_{adsorbed} \quad (1)$$

$$CoO + \text{Ph-Cl}_{adsorbed} \rightarrow \text{Ph-Cl}_{activated} \quad (2)$$

$$\text{Ph-Cl}_{activated} \rightarrow \text{Ph}^{\bullet} + \text{Cl}^{\bullet} \quad (3)$$

$$\text{Ph}^{\bullet} + O_{2adsorbed} \rightarrow CO_2 + H_2O \quad (4)$$

$$\text{Cl}^{\bullet} + \text{Cl}^{\bullet} \rightarrow Cl_2 \quad (5)$$

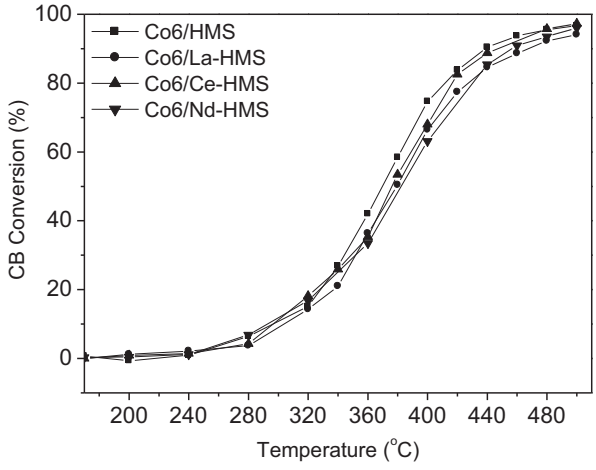

Fig. 19. Conversion curves of chlorobenzene catalytic combustion over Co/Ln-HMS.

For the step 1, the Ph-Cl molecule will be adsorbed by the supported Co_3O_4 active sites. Since the state of 3d orbits of Co^{2+} are half-filled ($3d^5$, five singled electron orbits) and there are six π-electrons in the benzene ring of adsorbed Ph-Cl, in order to make the 3d orbits of Co^{2+} to be filled, five π-electrons will be needed to delocalize from benzene ring into the 3d orbits of Co^{2+} to form ten electrons delocalization (here, the procedure is some what like that of dicyclopentadienyl iron and the 10 electrons also meet the $4n+2$ Hückel rule). As a result, the remaining one π-electron becomes instable and transform from the delocalization state into the localization state. Then, it will capture one electron from the C—Cl bond to form duplet. In addition, the weak hydrogen bond (O—H···Cl) between —OH of HMS and Cl of adsorbed Ph-Cl probably plays some role to weaken the C—Cl bond at this time also. Hence, the Ph• and Cl• will be formed. In step 4, the formed Ph• will be oxidized by the nearby adsorbed O_2 and the Cl• will combine with another Cl• which comes from other active sites to form Cl_2. In this step, Cl• may temporarily interact with Co^{3+} in the case that it could not meet another Cl• timely due to that the electron pair of Cl• could share with the empty orbits of Co^{3+}. The appearance of CeO_2 one aspect could result in the decrease of the size of Co_3O_4 and increase in the number of active sites (as mentioned above) the other aspect is that the Ce^{4+} empty orbits of 4f, 5d, 6s with different energy level is beneficial for the delocalization of π-electrons and the migration of Cl•.

4. Conclusions

Extra-framework and framework Ln modified Co/HMS were successfully prepared by post-loading and direct synthesis methods. All Ln modified Co/HMS samples keep the two-dimensional hexagonal mesostructure of HMS. It was found that the extra-framework Ce modified catalysts showed the better catalytic performance than the framework Ln modified ones due to the formation of CeO_2 which is advantagious to obtain the fine Co_3O_4 crystal clusters and the reduction of Ce^{4+} ions to Ce^{3+} species which will probably promote neighboring reduction of Co species. The suitable extra-framework Ce loading (6%, mass fraction) can effectively ameliorate the redox ability of Co species in the channel of HMS. Since the channel of HMS itself and $Co(NO_3)_3{\cdot}6H_2O$ aqueous solution both are hydrophilic, the diffusion and distribution of $Co(NO_3)_3{\cdot}6H_2O$ in HMS channel does not improve greatly by the framework Ln. However, the slightly improved redox ability and weak acidity originated from framework Ln still can do some contribution to the catalytic performance. Based on the analysis of electronic structure of Co and Ce, a tentative radical mechanism was proposed.

Acknowledgments

This work is supported by the projects of National Science Foundation for Distinguished Young Scholars of China (51125018), the Open Foundation of the State Key Laboratory of Comprehensive Utilization of Low-Grade Refractory Gold Ores (ZJKY2011(B)KFJJ002), the National Basic Research Program of China (2010CB732300) and the projects of Major Program of the National Natural Science Foundation of China (51090380).

Appendix A. Supplementary data

Supplementary data associated with this article can be found, in the online version, at http://dx.doi.org/10.1016/j.apcatb.2012.08.019.

References

[1] A. Khaleel, A.A. Nayli, Applied Catalysis B: Environmental 80 (2008) 176.
[2] S. Scirè, S. Minicò, C. Crisafulli, Applied Catalysis B: Environmental 45 (2003) 117.
[3] X.Y. Wang, Q. Kang, D. Li, Applied Catalysis B: Environmental 86 (2009) 166.
[4] Y. Shao, Z.Y. Xu, H.Q. Wan, H. Chen, F.L. Liu, L.Y. Li, S.R. Zheng, Journal of Hazardous Materials 179 (2010) 135.
[5] V. Jong, M.K. Cieplik, W.A. Reints, F.F. Reino, R. Louw, Journal of Catalysis 211 (2002) 355.
[6] F. Bertinchamps, A. Attianese, M.M. Mestdagh, E.M. Gaigneaux, Catalysis Today 112 (2006) 165.
[7] D.P. Debecker, F. Bertinchamps, N. Blangenois, P. Eloy, E.M. Gaigneaux, Applied Catalysis B: Environmental 74 (2007) 223.
[8] R.L. Fonseca, J.I.G. Ortiz, M.A.G. Ortiz, J.R.G. Velasco, Journal of Catalysis 209 (2002) 145.
[9] L. Becker, H. Forster, Journal of Catalysis 170 (1997) 200.
[10] Y. Dai, X.Y. Wang, D. Li, Q.G. Dai, Journal of Hazardous Materials 188 (2011) 132.
[11] F.S. Saleh, M.M. Rahman, Journal of Hazardous Materials 162 (2009) 1574.
[12] Y.L. Hao, B.C. Gates, Journal of Catalysis 263 (2009) 83.
[13] B.M. Choudary, S. Madhi, N.S. Chowdari, M.L. Kantam, B. Sreedhar, Journal of the American Chemical Society 124 (2002) 14127.
[14] W. Zhao, J.J. Li, C. He, L.N. Wang, J.L. Chu, J.K. Qu, T. Qi, Z.P. Hao, Catalysis Today 158 (2010) 427.
[15] A. Trovarelli, Catalysis Reviews: Science and Engineering 38 (1996) 439.
[16] B. Ernst, L. Hilaire, A. Kiennemann, Catalysis Today 50 (1999) 43.
[17] Q. Tang, Q. Zhang, P. Wang, H. Wan, Chemistry of Materials 16 (2004) 1967.
[18] P. Concepcion, C. Lopez, A. Martinez, V.F. Puntes, Journal of Catalysis 228 (2004) 321.
[19] P. Arnoldy, J.A. Moulijn, Journal of Catalysis 93 (1985) 38.
[20] B. Viswanathan, R. Gopalakrishnan, Journal of Catalysis 99 (1986) 342.
[21] L. Li, J. Lin, H.C. Zeng, Journal of Physical Chemistry B 104 (2000) 1783.
[22] F. Kapteijn, L. Singoredjo, A. Andreini, Applied Catalysis B: Environmental 3 (1994) 173.
[23] F. Arena, T. Torre, C. Raimondo, A. Parmaliana, Physical Chemistry Chemical Physics 3 (2001) 1911.
[24] M. Wu, X.Y. Wang, Q.G. Dai, Y.X. Gu, D. Li, Catalysis Today 158 (2010) 336.
[25] A. Trovarelli, C. de Leitenburg, M. Boaro, G. Dolcetti, Catalysis Today 50 (1999) 353.
[26] C. Li, Q. Xin, Journal of Physical Chemistry 96 (19) (1992) 7714.
[27] B.D. Cullity, Elements of X-ray Diffraction, third ed., Addison-Wesley, Reading, MA, 1978.
[28] S.T. Hussain, A. Sayari, F. Larachi, Applied Catalysis B: Environmental 34 (2001) 1.
[29] S. Krishnamoorthy, J.A. Rivas, M.D. Amiridis, Journal of Catalysis 193 (2000) 264.
[30] A.V. Boix, S.G. Aspromonte, E.E. Miró, Applied Catalysis A: General 341 (2008) 26.